JOURNAL OF CATALYSIS **179,** 100–110 (1998)
ARTICLE NO. CA982137

Crystallization Behavior of Tungstate on Zirconia and Its Relationship to Acidic Properties

II. Effect of Silica

Raymond A. Boyse[1] and Edmond I. Ko[2]

Department of Chemical Engineering, Carnegie Mellon University, Pittsburgh, Pennsylvania 15213-3890

Received December 2, 1997; revised April 1, 1998; accepted April 28, 1998

Zirconia–silica–tungstate aerogels were prepared by sol–gel chemistry followed by supercritical drying. The materials were characterized using nitrogen adsorption, X ray diffraction, Raman and DRIFT spectroscopy, and *n*-butane isomerization. Using the technique of prehydrolysis, we explored the role of silica, and the degree to which it was mixed with zirconia on the catalytic and acidic properties. The presence of silica, both dispersed in zirconia (well mixed) and segregated on the surface of zirconia (poorly mixed), retarded sintering caused by heat treatment, thereby increasing the surface area of the aerogels. On poorly mixed zirconia–silica, tungstate effectively dispersed onto the surface regardless of the existence of silica-rich patches. The ensuing reduction in specific activity in *n*-butane isomerization, compared to zirconia–tungstate, established that tungstate on these patches did not enhance active sites. On well-mixed zirconia–silica, the presence of siloxane species in the support further reduced catalytic activity by extending the influence of silica in zirconia–tungstate. The lower catalytic activities of these materials correlated with the presence of weaker Brønsted acid sites than those of zirconia–tungstate. This work demonstrates that silica as a dopant is effective in increasing the surface area of zirconia–tungstate but not in enhancing *n*-butane isomerization activity. © 1998 Academic Press

INTRODUCTION

Solid acid catalysts offer more environmentally friendly alternatives to conventional materials used in the chemical and petroleum industries (1). Among these alternatives of solid acids is the emerging class of metal oxides modified by dopants (2). Extensive research is available on several materials, particularly zirconia–sulfate which shows high activity at low temperatures in reactions requiring strong acidity such as cracking, alkylation, and isomerization (3, 4). More recently, zirconia–tungstate has received interest, for similar applications to zirconia–sulfate, because of its resistance to both dopant loss during thermal treatment and deactivation during catalytic reaction (5–13). Several examples of the potential of these materials are available: Fe- and Mn-promoted zirconia–sulfate exhibits very high activity at low temperatures in alkane isomerization (14); Pt-promoted zirconia–tungstate exhibits superior selectivity in isomerizations of larger alkanes such as *n*-heptane (8).

Several thorough studies exist to give a reasonably good understanding of zirconia–tungstate. Among these are studies focusing on the acidic properties of zirconia–tungstate (7), the catalytic behavior of the metal promoted material (8), and the structure of the dispersed surface tungstate (9). In our previous work with this material, we examined the effect of a range of preparation parameters on the catalytic and acidic properties (10). In particular, preparation method and activation temperature were found to play a dominant role in yielding a material active in *n*-butane isomerization. We established that the optimum activation temperature for a catalytically active material was strongly dependent on the preparation method. We corroborated the requirement that saturation coverage on the surface was ideal for an *n*-butane active material—attaining this coverage, however, was a strong function of preparation method, tungstate loading, and activation temperature. After the correct parameters were chosen to disperse a *monolayer* of tungstate on the surface of zirconia, the material became catalytically active in *n*-butane isomerization. Finally, the observed activity corresponded to the presence of increased Brønsted acid strength generated by the same active tungstate species regardless of preparation parameters. The possibility of enhancing the surface area or the active site density of zirconia–tungstate has motivated other studies, for example, on the role of extra anionic dopants on zirconia–tungstate (15). In this work, we look at the effect of modifying the underlying zirconia support with silica. We chose silica because of its potential in enhancing the surface

[1] Present address: Merck Sharp & Dohme Ltd., Ballydine, Kilsheelan, Clonmel, Co. Tipperary, Ireland.

[2] To whom correspondence should be addressed. Present address: City University of Hong Kong, Tat Chee Avenue, Kowloon, Hong Kong. Ph: 852-2788-9966. Fax: 852-2788-9922. E-mail: edko@cityu.edu.hk.

0021-9517/98 $25.00
Copyright © 1998 by Academic Press
All rights of reproduction in any form reserved.

area caused by the inhibition of sintering and in changing acid site distribution caused by interactions between cations with different electronegativities (16, 17).

To determine the role of silica on zirconia–tungstate, we used sol–gel chemistry to prepare zirconia–silica supports of differing homogeneity enabling us to determine the importance of silica distribution on the final properties (17, 18). Contrasting with coprecipitation techniques, sol–gel chemistry enables better control over the mixing of the two components. The standard alkoxide route yields a zirconia–silica support whereby zirconia particle formation precedes the formation of silica—in essence yielding a poorly mixed oxide with segregated zirconia and silica regions (16, 17, 19). Using the sol–gel technique of prehydrolysis promotes mixing of the metal alkoxides on a molecular scale and forms a more homogeneous material. In this manner, we can deliver zirconia–silica supports that are both well mixed or poorly mixed. This approach allows study of the effect of silica as a bulk oxide and as a dispersed oxide on the acidity of zirconia–silica promoted with tungstate and, consequently, a better understanding of the interactions between silica and tungstate and their mutual effects on the chemical properties of zirconia.

EXPERIMENTAL

Sample Preparation

Zirconia–silica–tungstate aerogels were prepared by incipient wetness impregnation of zirconia–silica aerogel supports with an aqueous solution of ammonium metatungstate (10, 17). We prepared zirconia–silica aerogels using zirconium *n*-propoxide and tetraethylorthosilicate precursors in the presence of a small amount of nitric acid, followed by drying in carbon dioxide under supercritical conditions (17). The zirconia–silica supports were prepared by both prehydrolyzed (PH) and nonprehydrolyzed (NPH) methods to explore the effect of support homogeneity on the final properties (17, 18). The sol–gel parameters used in preparing the aerogels are summarized in Table 1.

In the nonprehydrolyzed preparation of zirconia–silica–tungstate aerogels, we added 12.6 ml zirconium *n*-propoxide (70 wt% in propanol, Alfa) and 1.56 ml tetraethylorthosilicate (TEOS, Aldrich) to a solution of 15 ml 1-propanol (Fisher) and 1.05 ml HNO_3 (70% w/w, Fisher). The nominal silica loading was 20 mol% Si. This loading level was large enough to have an impact on the surface area but not so large as to inhibit the crystallization of zirconia into the tetragonal phase, desired for catalytic activity (3). In a second beaker, 1.25 ml distilled water was mixed with 15 ml 1-propanol. The contents of the second beaker were rapidly added to the first beaker until gelation occurred, which was recognized with the disappearance of the vortex caused by stirring. The exact time between mixing and gelation was recorded in Table 1 as the gel time. The product alcogel was aged for 2 h at room temperature before displacement of the alcohol solvent by carbon dioxide under supercritical conditions. In an autoclave operating at about 343 K and 20×10^3 kPa, the alcohol was displaced from the alcogel in approximately 2 h. The product aerogel was ground into a powder to pass through 100 mesh. Subsequent drying consisted of heating at 383 K under a vacuum for 3 h to remove water, followed by heating at 523 K under a vacuum for 3 h to remove residual organics and nitrates. Tungstate was incorporated, at two loadings of 10 and 14 wt% W, by impregnation to incipient wetness of the X ray amorphous powder with an aqueous solution of ammonium metatungstate hydrate (Aldrich). These loadings were guided by our previous work on zirconia–tungstate aerogels (10) to afford meaningful comparisons of acidic and catalytic properties. The materials were then dried under vacuum at 383 K for 3 h followed by calcination in flowing oxygen (27 l/h) for 2 h at a temperature in the range 1073 to 1223 K referred to as the activation temperature. We denote these materials, with 10 and 14 wt% W, as 20Si–10W and 20Si–14W, respectively.

The final aerogel was prepared by using a *prehydrolyzed* zirconia–silica also containing 20 mol% Si. In the prehydrolyzed preparation, a portion of the total water was mixed with the silicon precursor. The prehydrolysis ratio, defined as the molar ratio of water to silicon (mol H_2O/mol Si), was chosen as 2.7 to promote mixing of zirconia and silica on a molecular level (17). Briefly, we added 1.34 ml TEOS to a solution of 20 ml 1-propanol and 0.05 ml HNO_3 (70% w/w, Fisher) and 0.270 ml H_2O. The solution was stirred for 10 minutes before addition of 10.76 ml zirconium *n*-propoxide

TABLE 1

Sol–Gel Parameters for Zirconia–Silica–Tungstate Aerogels[a]

Sample	Water ratio[b] (mol H_2O/mol M)	Acid ratio (ml acid/mol M)	PH water ratio[b] (mol H_2O/mol Si)	PH acid ratio (ml acid/mol Si)	Gel time (s)
20Si–10W	2.70	29.9	0.0	0.0	53
20Si–14W	2.70	29.9	0.0	0.0	65
20Si(PH)–14W	2.85	35.7	2.7	8.5	131

[a] All gels prepared in 30 ml alcohol.
[b] Nomenclature: PH = prehydrolyzed; M = metal atoms.

and the remaining 1.02 ml HNO_3. In a second beaker, 0.81 ml distilled water was mixed with 15 ml 1-propanol. The contents of the second beaker were added to the first beaker to yield an alcogel. Supercritical drying, vacuum drying and calcination procedures were identical to those followed for the non-prehydrolyzed materials. Tungstate (14 wt% W, nominal) was added by incipient wetness impregnation. We designate this sample 20Si(PH)–14W.

Sample Characterization

Textural, structural, acidic, and catalytic properties were examined for each of the samples. Textural characterization was determined by nitrogen adsorption using an Autosorb-1 gas sorption system (Quantachrome Corp.). Samples were outgassed at 383 K, under vacuum, for 2 h prior to analysis. Forty point desorption isotherms were obtained, from which the BET surface area, total pore volume, and pore size distribution were calculated. Zirconia and tungsten oxide crystal phase determinations were made from X ray powder diffraction (XRD) patterns obtained using a Rigaku D/max diffractometer with Cu K_α radiation. Crystalline tungsten oxide was further monitored using Raman spectroscopy. Laser Raman spectra were recorded using a Spex 1403 0.85 m double spectrometer. The 488 nm line of a Spectra-Physics model 2020 Argon ion laser was used for excitation. Spectra were gathered from samples contained in glass vials, under ambient conditions, over the range 200–1200 cm^{-1} with a spectral slit width of 600 μm and step size of 2 cm^{-1}. Differential thermal analysis (DTA) was performed on a Perkin-Elmer DTA 1700 thermal analyzer with thermal analysis data station. Thermogravimetric (TG) analysis was performed on a Cahn 113 Thermogravimetry Microbalance monitored by a Cahn 2000 Recording Electrobalance. In both DTA and TG experiments, approximately 60 mg samples were heated at a rate of 10 K/min from room temperature to 1273 K under flowing helium (3 l/h).

Catalytic activities were determined using a differential, downward flow, tubular fixed bed reactor of 0.5 inch diameter, operated at atmospheric pressure. Approximately 0.5 g of sample was pretreated at 588 K for 1 h under 2.4 l/h (40 sccm) flowing helium. The sample was then cooled to 553 K and exposed to a feed stream mixture of 0.06 l/h (1 sccm) *n*-butane (Matheson, Research Grade) in 0.60 l/h (10 sccm) hydrogen (Matheson UHP). A Gow-Mac 550P gas chromatograph with thermal conductivity detector (Column: Supelco 23% SP 1700 on 80/20 Chromosorb, 1/8 in. $\times$ 30 ft) was used to determine the composition of the product stream. The reactions were run differentially at conversions of less than 5%. Isobutane was the only observed product over zirconia–silica–tungstate aerogels indicating that cracking or reforming reactions were negligible under these conditions. We note that trace amounts of propane were observed during reaction over the most active zirconia–tungstate aerogels. The reaction rates were calculated as specific activity using the experimentally determined surface area at each calcination temperature.

Diffuse reflectance infrared Fourier transform (DRIFT) spectroscopy was employed to study the silica species on the materials. The experiments were carried out on a Mattson Galaxy 5020 FT-IR, with a DTGS detector and a Harrick diffuse reflectance attachment (DRA-2). Additionally, in situ DRIFT spectroscopy of adsorbed pyridine was accomplished using a Harrick reaction chamber (HVC-DR2) (20). Each spectrum was acquired by averaging 128 scans taken over the range 400–4000 cm^{-1} at a resolution of 2 cm^{-1}, obtained from samples diluted in KBr. Ex situ spectra were acquired under ambient conditions, whereas in situ DRIFT spectra were acquired under flowing helium. Under in situ conditions, samples were pretreated at 588 K for 15 minutes, similar conditions to those used in the isomerization of *n*-butane, after which a spectrum was collected. The type and strength of acidity on the surface was measured by cooling the samples to 373 K and subsequently exposing them to pyridine for 15 minutes by diverting the helium flow through a pyridine saturator. Spectra were then taken at 373, 423, 473, 553, and 623 K after 10 minutes in flowing helium at each temperature. The *type* of surface acidity was determined by the peaks at 1445 and 1490 cm^{-1} (21, 22). Relative populations of Brønsted and Lewis sites were calculated by the method of Basila and Kantner (23) using the integrated areas under the previously mentioned peaks. The relative *strength* of the acid sites was determined by monitoring the effect of temperature on the peaks at 1445 and 1490 cm^{-1}. Materials with stronger Brønsted acid sites retained irreversibly adsorbed pyridine up to higher temperatures.

RESULTS

Textural Properties of Zirconia–Silica–Tungstate Aerogels

The roles of support homogeneity, tungstate loading, and activation temperature on the textural properties were examined using nitrogen adsorption. The zirconia–silica–tungstate aerogels possessed surface areas in the range of 78–94 m^2/g after activation at 1073 K (see Table 2). The corresponding area of zirconia–tungstate aerogel, with 10 wt% W prepared by the same method, was 73 m^2/g (10). The higher surface area, attributed to the presence of silica, demonstrated that silica further prevented the deterioration of surface area caused by sintering due to heat treatment. These areas were significantly higher than those of a pure zirconia aerogel, which retains a surface area of about 40 m^2/g after calcination at 1073 K (24), caused by the added resistance to sintering associated with dopants. Table 2 also shows that both of the aerogels with nonprehydrolyzed supports, 20Si–10W and 20Si–14W, clearly maintained higher surface area than sample 20Si(PH)–14W with the

TABLE 2

Textural Properties of Zirconia–Silica–Tungstate Aerogels

Sample	Activation temperature (K)	Loading[a] (W-units/nm^2)	Pore volume (cm^3/g)	Surface area (m^2/g)
20Si–10W	773	2.23	0.46	163
	1073	3.87	0.38	94
	1123	4.38	0.37	83
	1173	5.51	0.36	66
	1223	11.03	0.25	33
20Si–14W	773	3.27	0.51	163
	1073	5.99	0.41	89
	1123	7.62	0.38	70
	1173	10.66	0.33	50
	1223	15.24	0.28	35
20Si(PH)–14W	773	3.63	0.48	147
	1073	6.84	0.40	78
	1123	7.96	0.38	67
	1173	11.59	0.34	46
	1223	15.68	0.29	33

[a] Calculation based on the experimentally determined surface areas and assuming each W-unit occupied 0.16 nm^2.

prehydrolyzed support. Previous research has established the less effective extent to which a well-mixed zirconia–silica, prepared by prehydrolysis, resists surface area loss with increasing heat treatment (16, 17). Hence, the lower surface area of 20Si(PH)–14W was a direct consequence of the homogeneous nature of the zirconia–silica support. The pore volumes of the aerogels were in the range 0.38–0.41 cm^3/g after activation at 1073 K, which was higher than zirconia–tungstate aerogel's value of about 0.29 cm^3/g. The aerogels were mesoporous with average pore sizes of 9–10 nm, whereas the prehydrolyzed material 20Si(PH)–14W possessed a much broader distribution of pore sizes due to the well-mixed nature of the support (16).

Figure 1 shows the effect of activation temperature on the surface areas of samples 20Si–10W, 20Si–14W and 0Si–10W, the pure zirconia–tungstate aerogel. Zirconia–tungstate showed a continuing surface area loss with respect to activation temperature. The equivalent sample with silica, 20Si–10W, also shows a similar loss up to a temperature of 1223 K, whereupon a relatively sharp loss in area was observed. Sample 20Si–14W demonstrated the exact same behavior except that the sharp area loss occurred at the lower activation temperature range of 1123–1173 K. Both of these sharp losses corresponded to the formation of crystalline WO_3 as identified by X ray diffraction. Hence the crystallization of WO_3 was concurrent with an accelerated loss in surface area, probably caused by plugging of the pores (11), illustrating that zirconia–silica–tungstate retained the highest surface area when tungstate was dispersed on the surface.

Structural Properties of Zirconia–Silica–Tungstate Aerogels

The effect of silica, and the extent to which it was mixed with zirconia, was further evident in the structural properties of the support and the surface tungstate. Differential thermal analysis monitored the tetragonal-to-monoclinic transformation of the aerogels. This phase transformation was accompanied by a decomposition of organic species associated with alkoxide-based materials observed in thermogravimetric analysis, allowing TG to monitor the crystallization of zirconia as well as the thermal stability of the dopants. Samples 20Si–10W and 20Si–14W remained X ray amorphous up to 1113 K during a 10 K/min heat ramp as opposed to 893 K for zirconia–tungstate. These observations established that zirconia–silica–tungstate remained X ray amorphous to even higher temperatures than zirconia–tungstate. Using XRD, we monitored the phase transformation of both zirconia and tungsten oxide. As shown in Fig. 2, the existence of an X ray peak at $2\theta \approx 30^\circ$ verified the presence of tetragonal zirconia in all the samples with calcination at 1073 K. Figure 2 also demonstrates that the samples remained in the tetragonal phase of zirconia with activation up to 1223 K. Activation above this temperature resulted in the tetragonal-to-monoclinic transformation of zirconia, evident in the XRD pattern in Fig. 2 for sample 20Si–10W.

The emergence of crystalline WO_3 with increasing activation temperature was recognized by three peaks in the XRD pattern in the range $2\theta \approx 23$–25°. Figure 2 shows the formation of WO_3 on sample 20Si–14W and 20Si–10W at activation temperatures of 1173 and 1223 K, respectively. Previous research suggests that WO_3 forms on zirconia

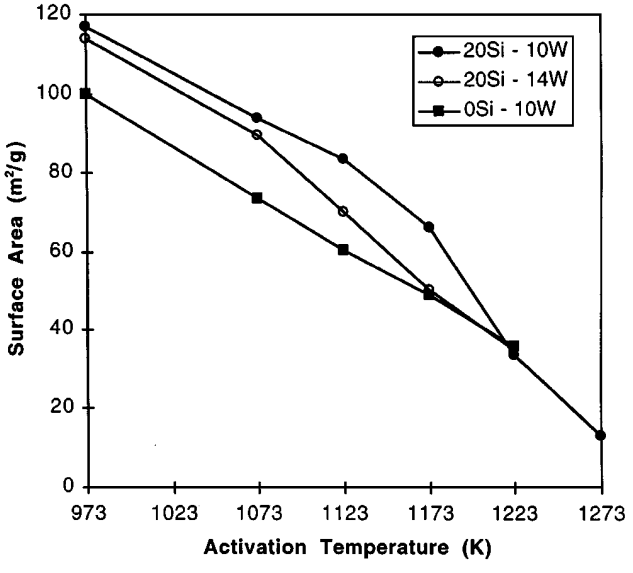

FIG. 1. Effect of heat treatment (calcination for 2 h at the temperatures indicated) on the BET surface areas of aerogels 0Si–10W, 20Si–10W, and 20Si–14W.

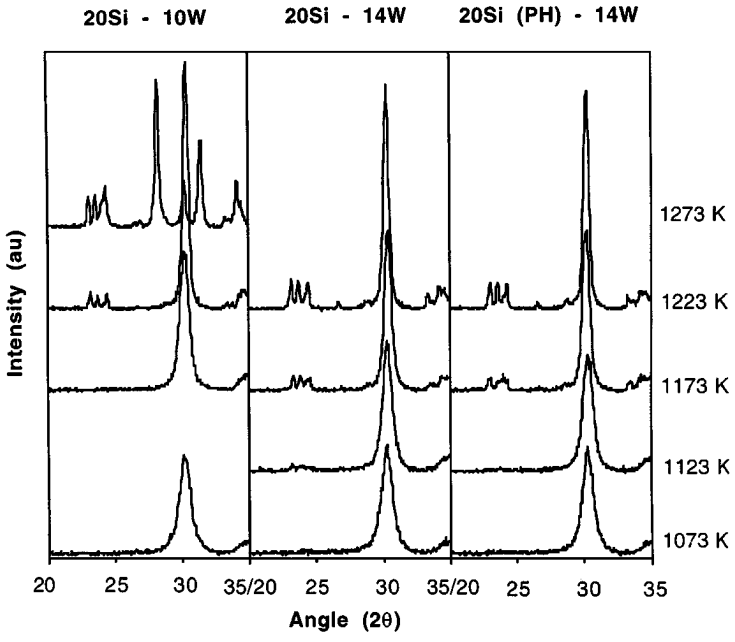

FIG. 2. X-ray diffraction patterns for samples 20Si–10W, 20Si–14W, and 20Si(PH)–14W as a function of activation temperature. Metastable tetragonal (T) zirconia indexed by a peak at $2\theta \approx 30^\circ$, crystalline WO_3 by peaks at $2\theta \approx 23$–25°.

and is detectable by XRD, above theoretical monolayer coverage, which occurs as tungstate surface density increases as a result of sintering of the underlying zirconia (10). Table 2 illustrates that the emergence of WO_3 was identified by XRD at surface loadings in the range 10.7–11.0 W-units/nm^2—loadings which were indeed in excess of a single monolayer approximated at 6.25 W-units/nm^2 (10). The activation temperature resulting in WO_3 crystallization was lower for 20Si–14W than 20Si–10W because less surface area reduction caused by retarded sintering of the underlying support was necessary for monolayer coverage to be exceeded in the former sample that had more tungstate. Figure 2 demonstrates that the prehydrolyzed sample 20Si(PH)–14W exhibited WO_3 peaks after activation at 1173K similar to the nonprehydrolyzed sample 20Si–14W with the same tungstate loading. Hence, formation of WO_3 was primarily a function of tungstate loading in relation to the surface area of the underlying support.

A more detailed assessment of tungstate structure was possible using Raman spectroscopy. Figure 3 shows the effect of activation temperature on the Raman spectra for samples 20Si–10W, 20Si–14W, and 20Si(PH)–14W. Because of a high Raman scattering cross-section, smaller WO_3 crystallites are detectable by Raman than XRD (9, 27). Figure 3a shows the emergence of WO_3, evident by peaks at 805 and 715 cm^{-1}, on sample 20Si–10W at an activation temperature of 1173 K. This temperature was lower than that determined by XRD and corresponded to a surface loading significantly closer to that of approximately one monolayer. Figure 3b, c shows similar spectra for samples 20Si–14W and 20Si(PH)–14W. Both samples possessed WO_3 after activation at 1123 K which corresponded to surface loadings in the range 7.6–8.0 W-units/nm^2. Again, tungsten oxide crystallization occurred in the vicinity of monolayer coverage, and *remained unaffected by the presence or distribution of silica.*

Figure 4 shows the ex situ DRIFT spectra of each of the zirconia–silica–tungstate aerogels to allow further insight into the structure of the materials. The emergence of a peak at 750 cm^{-1} corresponded to the formation of crystalline WO_3 observed in XRD patterns. Symmetric and asymmetric Si–O–Si vibrations were observed in all samples at 805–830 and 1000–1250 cm^{-1}, respectively. Deconvolution of the band at 1000–1250 cm^{-1} into two bands representing the transverse and longitudinal mode of asymmetric Si–O–Si vibrations is given in Table 3. We observe that the transverse mode, designated peak II, consistently shifted to higher wavenumbers with increasing activation temperatures. This trend, evident in each of the materials shown in Fig. 4, was associated with an increasingly stronger silica network (28, 29). The implications of this network strengthening are discussed later in more detail.

Catalytic and Acidic Properties of Zirconia–Silica–Tungstate Aerogels

The zirconia–silica–tungstate aerogels were probed for catalytic activity over strong acid sites by the isomerization of *n*-butane in H_2 at 588 K. The samples exhibited no noticeable deactivation with time-on-stream—the activity during reaction over a 90-min time period deviated by less than 0.025 μmol/m^2/h from the steady-state or average activity. Repeated examination of a test sample (with ex situ recalcination at 773 K in oxygen between reactions) demonstrated

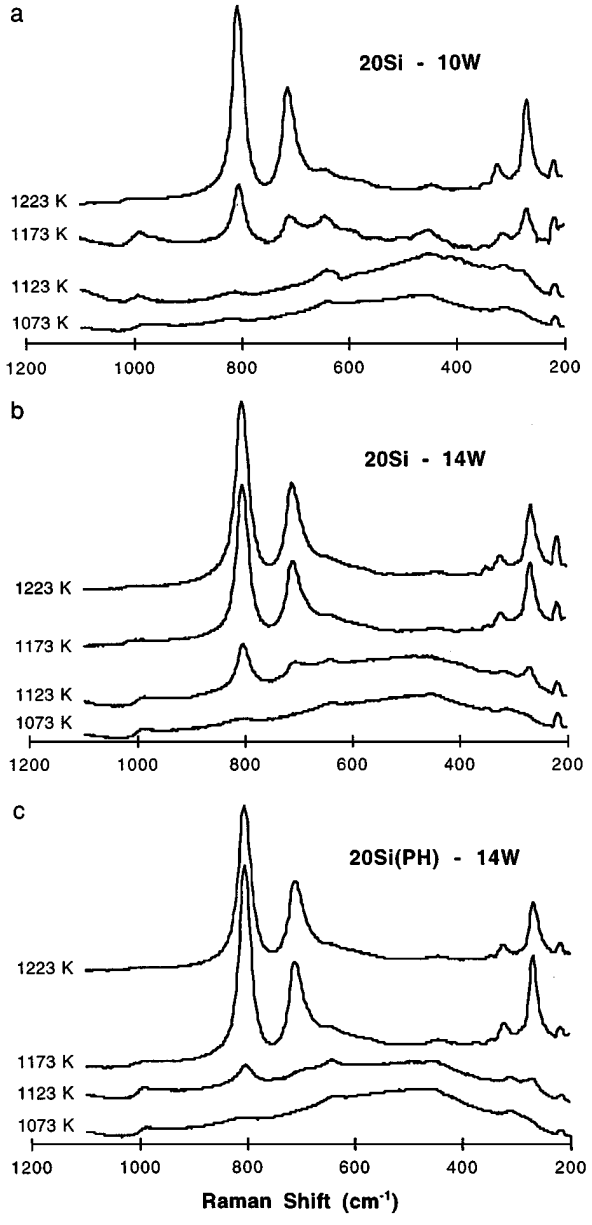

FIG. 3. Raman spectra for samples (a) 20Si-10W, (b) 20Si-14W, and (c) 20Si(PH)-14W as a function of activation temperature. Peaks at 805 and 715 cm^{-1} are indexed to crystalline WO_3.

that a loss in the catalytic activity did not occur, and that the activity remained in a window of about 0.15 μmol/m^2/h, which was about 10% of the maximum observed specific rate. Figure 5 shows the dependence of steady-state activity on activation temperature for all of the aerogels. Reported activation temperatures for maximum activity in this reaction are in the range 1073–1123 K (5, 6). The most active aerogel was 0Si–10W—the material without silica. The optimum activation temperature for maximum catalytic activity was at 1123 K. This temperature corresponded to saturation coverage of zirconia, as observed by the onset of WO_3 formation by Raman spectroscopy, which occurred at about theoretical monolayer coverage (10). Sample 20Si–10W had the same tungstate loading as sample 0Si–10W, but the optimum activation temperature was shifted to the higher temperature of 1223 K. The maximum activity also occurred at saturation coverage, which was attained with activation at 1173–1223 K as determined by Raman spectroscopy and XRD, respectively. Hence, the catalytic activity was highest with maximum coverage of the support surface by dispersed tungstate and did not occur in the typical temperature range found in the literature (5, 6, 8) as a result of the increased surface area of this mixed oxide

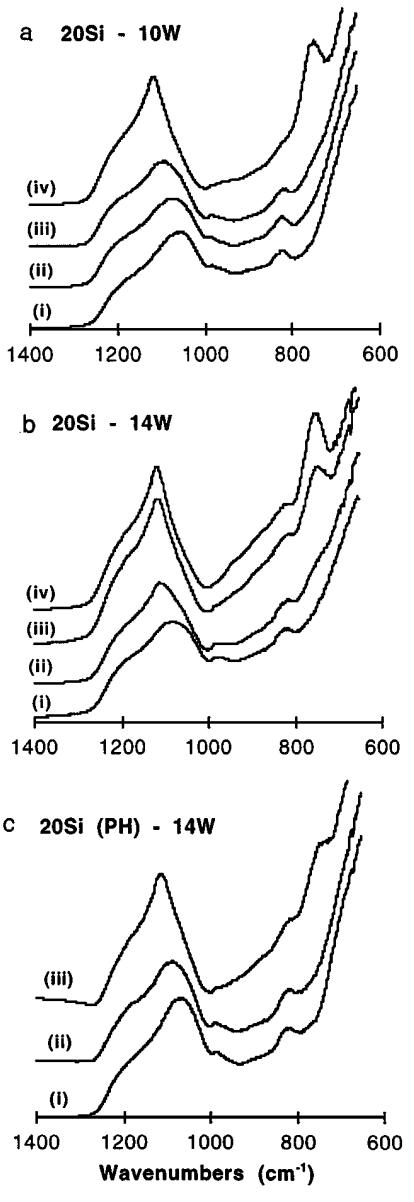

FIG. 4. Ex situ DRIFT spectra for samples (a) 20Si–10W, (b) 20Si–14W, and (c) 20Si(PH)-14W as a function of activation temperatures (i) 1073 K, (ii) 1123 K, (iii) 1173 K, and (iv) 1223 K. Peaks from 1000 to 1250 cm^{-1} are indexed to Si–O–Si asymmetric vibrations.

TABLE 3

Ex Situ Si–O–Si Deconvoluted Peak Locations with Respect to Activation Temperature

Sample	1073 K		1123 K		1173 K		1223 K	
	I[a]	II[b]	I	II	I	II	I	II
20Si–10W	1188	1060	1200	1080	1208	1102	1204	1116
20Si–14W	1204	1082	1208	1107	1207	1116	1204	1118
20Si(PH)–14W	1200	1076	1199	1092	1203	1117	—	—

[a] Longitudinal mode of asymmetric Si–O–Si vibration given in wavenumbers (cm^{-1}).

[b] Transverse mode of asymmetric Si–O–Si vibration given in wavenumbers (cm^{-1}).

support. By increasing the tungstate loading to 14 wt% W, Fig. 5 shows that the activity profiles for samples 20Si-14W and 20Si(PH)–14W both have maximum catalytic activity at 1123 K—the points of WO_3 formation as seen by Raman spectroscopy. Both samples had lower specific activities than the nonsilica sample 0Si–10W, suggesting that the presence of silica (i) resulted in a decrease in the active site density or (ii) weakened the existing acid sites on the surface of zirconia.

The acidic properties of samples 20Si–14W and 20Si(PH)–14W activated at 1123 K were determined using DRIFT spectroscopy of adsorbed pyridine. We verified the existence of (i) Lewis acid sites by peaks at 1610 and 1447 cm^{-1} and of (ii) Brønsted acid sites by peaks and 1540 and 1490 cm^{-1}. The materials possessed both Lewis and Brønsted acid sites similar to zirconia–tungstate as established by peaks at 1490 and 1447 cm^{-1}. Table 4 shows the relative strength of the Brønsted acidity which was ascertained by monitoring the effect of temperature on the peak at 1490 cm^{-1}. For sample 20Si–14W, irreversibly adsorbed pyridine was observed on the surface at 553 K, but not at 623 K. We previously observed that pyridine was retained on catalytically active zirconia–tungstate up to temperatures of 623 K (10). This temperature is very similar to that reported elsewhere to which pyridine remains irreversibly adsorbed on zirconia-tungstate (25, 30). Hence, the silica containing sample, 20Si–14W, possessed sites of lesser strength to zirconia–tungstate. Sample 20Si(PH)–14W also adsorbed pyridine at 553 K, but the infrared signature of pyridinium ion was weaker, suggesting that this sample contained (i) weaker sites than zirconia–tungstate and (ii) fewer sites than 20Si–14W. We note in passing that these temperatures are not high enough for pyridine decomposition rather than desorption (25).

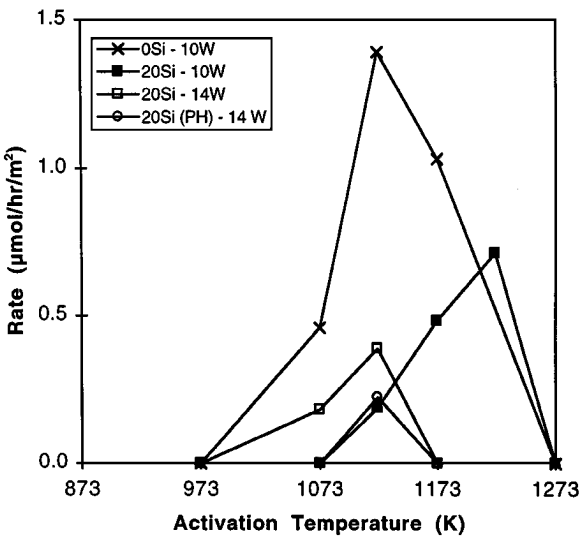

FIG. 5. Steady-state *n*-butane isomerization activity as a function of activation temperature (after 70 min time-on-stream) for samples 0Si–10W, 20Si–10W, 20Si–14W, and 20Si(PH)–14W. Samples were calcined in flowing oxygen for 2 h at the temperatures indicated.

TABLE 4

Catalytic and Acidic Properties of Aerogels Activated at 1123 K

Sample	Catalytic activity (μmol/m^2/h)	Temperature range of pyridine desorption from Brønsted acid sites[a]
0Si–10W	1.39	623–673 K[b]
20Si–14W	0.39	553–623 K
20Si(PH)–14W	0.22	553–623 K

[a] Determined by pyridine FT–IR spectroscopy.

[b] From Ref. 10.

DISCUSSION

Previous studies of zirconia–tungstate based materials demonstrate that the synthesis of a strong solid acid, active in reactions such as alkane isomerizations, requires the presence of a crystalline zirconia support (3, 4) promoted with dispersed tungstate (8, 10). Standard parameters recommended to produce this material are loadings of about 10–12 wt% W (6, 8) with calcination in the temperature range 1073–1123 K (5–10). Under these circumstances, thermal treatment induces support crystallization followed by solid–solid wetting of zirconia by tungstate to surface saturation coverage (6, 8). In this work, we explored the possibility of enhancing zirconia–tungstate by adding silica to produce aerogels of higher surface areas and, in the process, have gained insight into the relative importance of variables such as support homogeneity, tungstate loading, and activation temperature.

The addition of 20 mol% Si during the preparation of zirconia–tungstate yielded a material, sample 20Si–10W, with a surface area of 94 m^2/g after activation at 1073 K (Table 2). The measured surface area for sample 0Si–10W, which did not contain silica, was 73 m^2/g at the same activation temperature (10)—differences between areas were above the experimental error of approximately 5%. It

appeared that the role of silica in the enhancement of textural properties was to stabilize ZrO_2 against sintering caused by heat treatment (3, 10). Thermal analysis established that crystallization of 20Si–10W occurred at a significantly higher temperature than 0Si–10W, thus verifying that the thermal stability imparted to ZrO_2 by tungstate was further enhanced by the presence of silica. In addition to affecting texture, Fig. 5 illustrates that the presence of silica also changed the catalytic behavior of 20Si–10W with respect to 0Si–10W. Sample 20Si–10W attained maximum catalytic activity after calcination at 1223 K, contrasting with the optimum activation for sample 0Si–10W of 1123 K. The significant difference in the optimum activation temperature was explained by recalling that the requirement for optimum activity is saturation coverage of zirconia by tungstate (8, 10). For example, saturation coverage on 0Si–10W occurred after activation at 1123 K (10): this treatment induced the appropriate surface area loss, by sintering of the underlying support, to give approximately monolayer coverage of zirconia (estimated at a loading of 6.25 W-units/nm^2). We note in passing that the term *monolayer coverage* was used to represent the amount of tungstate on zirconia–silica with respect to the experimentally determined surface area. This term has proved useful here and in previous work (10) because it consistently approximated the point at which *maximum* catalytic activity occurred. However, the term is not meant to represent the actual structure of dispersed tungstate on the support, which very likely does not exist as an actual monolayer (8, 30). In other words, our results do not rule out small clusters of tungsten oxide, especially at low loadings, as the catalytically active species.

In this study, sample 20Si–10W retained a higher surface area than a typical zirconia–tungstate material because of the presence of silica. Table 2 verifies that theoretical monolayer coverage was attained with calcination in the range 1173–1223 K corresponding to a surface-loading range of 5.5–11.0 W-units/nm^2. Hence, the necessity for a higher activation temperature for sample 20Si–10W corroborated the relationship between maximum catalytic activity and saturation coverage of the support. At 1123 K, there simply was not enough tungstate to cover the surface of this support, thus there was a fraction of the support not contributing to catalysis. Because the data in Fig. 5 were calculated using *total* support surface area, there was an apparent shift in the activation profile of 20Si–10W.

Other possible factors that may alter catalytic behavior include the crystal phase of ZrO_2 which has been associated with the generation of strong acid sites responsible for catalytic activity (3, 6, 19, 26). XRD patterns in Fig. 2 verified that sample 20Si–10W exhibited the tetragonal phase of zirconia over the entire activation range tested and was therefore not responsible for the changing activity profile. However, we note that silica loadings higher than 20 mol% Si may prevent support crystallization thereby having an adverse effect on catalytic activity (19). For example, Miller and Ko observed that zirconia–silica with 50 mol% Si is X ray amorphous after activation at 973 K and exhibits only a weak crystal structure at 1173 K (17).

The necessity for complete coverage on the higher surface area zirconia–silica prompted an increase in tungstate loading from 10 to 14 wt% W to maximize activity at a lower activation temperature. Table 2 demonstrates that sample 20Si–14W attained theoretical monolayer coverage after activation between 1073 and 1123 K recognized by an increase in surface tungstate density from 5.99 to 7.62 W-units/nm^2. Figure 3 verified that the onset of WO_3 formation, corresponding to a Raman peak at 805 cm^{-1}, occurred in this temperature range. Referring to the catalytic profile in Fig. 5, we see that the optimum activation temperature shifted from 1223 to 1123 K, as expected, by increasing tungstate loading. The role of loading on stability was clarified by comparison of 20Si–10W and 20Si–14W: activation at 773 and 1073 K generated materials with very similar surface areas (Table 2) despite different tungstate loadings. Above 1123 K, tungstate loading became an important factor because it controlled the activation temperature associated with the onset of surface area loss concurrent with WO_3 crystallization. Apparently, as long as tungstate remained dispersed, implied by a lack of Raman peaks at 805 cm^{-1} indicative of WO_3, the loading did not modify noticeably the resistance of zirconia–silica to sintering.

From the discussion so far, it is evident that the addition of silica did not alter the crystallization behavior of tungstate. On the other hand, changes in activity and acidity inferred that some interaction was taking place between the dopants. To elucidate the interactions between each of the components, we present a schematic model in Fig. 6 of samples 20Si–14W and 20Si(PH)–14W based on previous

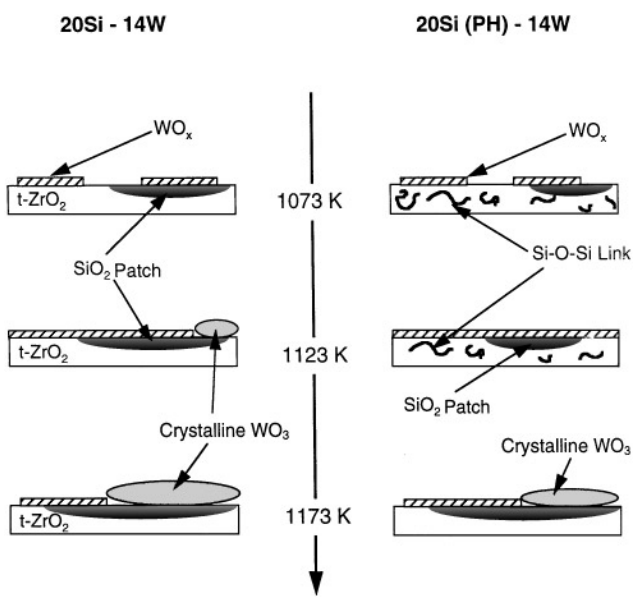

FIG. 6. Schematic models of 20Si-14W and 20Si(PH)-14W.

work with zirconia–silica mixed oxides (16, 17) and zirconia–tungstate supported oxides (10). The two samples possessed supports of different homogeneity. Miller and Ko demonstrated that control over mixing was afforded during the sol–gel preparation by a technique called prehydrolysis (16, 17). They concluded that *without* prehydrolysis, zirconia particles rapidly formed during the wet gel preparation, onto which silica was deposited. The resulting poorly-mixed zirconia–silica became the support for sample 20Si–14W, which after activation at 1073 K can be modeled schematically in Fig. 6 as a material with silica patches on the surface of zirconia. Increasing heat treatment induced growth of the silica patches by simultaneously augmenting (i) surface area loss by sintering and (ii) phase separation of zirconia and silica. Monaco and Ko reported that an increase in the frequency of the transverse mode of asymmetric Si–O–Si vibrations corresponds to growth of silica particles (28). Table 3 shows that sample 20Si–14W exhibited a peak II shift from 1082 to 1118 cm^{-1} with an increase in activation from 1073 to 1223 K. Hence, ex situ DRIFT data in Fig. 4 confirmed that the silica patches on zirconia got larger, covering a larger fraction of the surface, with increasing activation temperature as shown schematically in Fig. 6.

For sample 20Si–14W in Fig. 6, there was clear evidence of some interaction between silica and tungstate. X ray diffraction and textural data determined that both samples 20Si–10W and 20Si–14W contained only dispersed tungstate below theoretical monolayer coverages. The immediate implication of this observation was that WO_3 crystallization took place at about complete coverage of the zirconia–silica support, despite the presence of silica domains on the surface. Hence, we conclude that tungstate remained dispersed on the silica regions. This result is unexpected in light of the fact that tungstate and silica interact much more weakly than tungstate on other oxides such as alumina, zirconia, and titania. For example, WO_3 crystallizes on pure silica after activation at temperatures as low as 773 K (27). Because there was no premature crystallization of WO_3 below calcination at 1073 K, despite the presence of large patches of surface silica, tungstate on the silica patches clearly did not behave as tungstate would on bulk silica. In fact, it appeared that the silica patches were thin enough to allow the underlying zirconia to stabilize dispersed tungstate.

Even though we observed that tungstate evolved on zirconia–silica and zirconia in a similar manner, catalytic data in Fig. 5 illustrate that after optimum activation, both samples 20Si–10W and 20Si–14W were noticeably less active than sample 0Si–10W calcined at 1123 K. The apparent prerequisite for *n*-butane active samples has been the existence of well-dispersed tungstate on zirconia (8, 10). This raises a question: if tungstate remains dispersed on zirconia–silica, why is there an observed decrease in catalytic activity? Recall that pyridine remained irreversibly adsorbed on the surface of 20Si–14W at a temperature of 553 K. Meanwhile, we note that even though zirconia–tungstate, capable of adsorbing pyridine up to 553 K, is *n*-butane active, optimum activation generates a material capable of adsorbing pyridine up to 623 K (10). Hence, pyridine adsorption differentiated between *n*-butane active sites of two strengths: sites adsorbing pyridine up to 623 K which are highly active; sites adsorbing pyridine up to 553 K which are less so. In this work, sample 20Si–14W possessed Brønsted acid sites of reduced strength compared to those of zirconia–tungstate. Consequently, we observed a decrease in catalytic activity upon addition of silica. As shown in Fig. 6, 20Si–14W was a nonprehydrolyzed material containing 20 mol% Si consisting primarily of surface silica patches. Taking into account the preferential segregation of silica on the surface, we speculate that those sites participating in the isomerization were those least weakened by silica and therefore farthest away from the silica patches which resided over a large fraction of the zirconia–silica. Finally, the loss in catalytic activity upon increasing the activation temperature to 1173 K was probably caused by the combined emergence of WO_3 (which is inactive in *n*-butane isomerization) and growing silica patches on the surface of zirconia.

Considering the reduced activity resulting from silica-rich regions, one might anticipate that well-mixed zirconia–silica, with fewer silica patches on the surface interacting with tungstate, would be more catalytically active. To accomplish this outcome, we used *prehydrolysis* to disperse silica throughout the support yielding sample 20Si(PH)–14W. Briefly, during the formation of the zirconia–silica gel, prehydrolysis enables the monodispersed silicon precursor to form dimers and trimers before formation of zirconia primary particles (16). Hence, a prehydrolyzed support also possesses siloxane (Si–O–Si) links throughout the zirconia network, as depicted in Fig. 6. We verified the more homogeneous nature of 20Si(PH)–14W by analysis of the deconvoluted silica infrared peak from 1000–1250 cm^{-1} (peak II in Table 3). With calcination at 1073 K, peak II was positioned at 1076 cm^{-1} for 20Si(PH)–14W as opposed to 1082 cm^{-1} for 20Si–14W. Apparently, the Si–O–Si bonds contained in the siloxane species, resulting from the proximity of zirconium atoms, were weaker and resulted in a shift to lower frequency for the Si–O–Si band—the lower peak II frequency vibration was consistent with the presence of siloxane links. At the higher activation temperature of 1123 K, the peak positions for 20Si(PH)–14W and 20Si–14W were 1092 and 1107 cm^{-1}, respectively, indicating that dispersed siloxane species were still present in zirconia in the prehydrolyzed sample. At 1173 K, however, the similar infrared signatures evident in Fig. 4b, c implied that the prehydrolyzed and non-prehydrolyzed materials were identical in terms of silica distribution. In sum, sample 20Si(PH)–14W contained less *surface* silica than 20Si–14W in the temperature range 1073–1123 K.

Figure 5 clearly shows that 20Si(PH)–14W was less active than 20Si–14W despite the fact that it possessed both fewer silica-rich patches and fewer crystalline WO_3 (Fig. 3c). Thus, the low specific activity cannot be explained in terms of surface silica alone. We noted that XRD patterns and Raman spectra in Figs. 2 and 3 show the similar evolution of crystalline WO_3 on these samples—support homogeneity did not alter the behavior of surface tungstate. As expected, maximum activity occurred with activation at 1123 K at monolayer coverage of zirconia by dispersed tungstate. The reduction in *n*-butane activity was consequently assigned to the presence of dispersed siloxane links in the zirconia network. Although the exact role of these siloxane links was unclear, their manifestation on acidic properties was evidenced in pyridine FT–IR. Sample 20Si(PH)–14W (well mixed) activated at 1123 K retained irreversibly adsorbed pyridine up to 473 K, and possibly 553 K, but the pyridinium ion signature at this temperature was noticeably less than that of pyridinium ion on 20Si–14W (poorly mixed). The addition of dispersed silica, in the form of siloxane, therefore weakened the overall Brønsted acid strength, in a manner similar to silica patches in 20Si–14W. The weaker pyridinium ion signature at the same temperature of 553 K in conjunction with reduced catalytic activity indicated that the presence of siloxane reduced the number of catalytically active acid sites compared to 20Si–14W, but not the strength of the active sites. Therefore, we speculate that using prehydrolysis to disperse silica throughout the zirconia support increased the influence of silica on the acidity of zirconia–tungstate by enabling siloxane to affect those regions not in the immediate proximity of the surface silica patches.

Recent studies (7, 8, 30) have suggested that redox chemistry plays an important role in *n*-alkane isomerization over zirconia–tungstate. However, samples in these studies either contain platinum, which facilitates the reduction of tungsten species at about 440–500 K (8), or are treated in a reducing atmosphere prior to reaction (30). Thus, we cannot directly compare our zirconia–tungstate aerogels with these samples in terms of the reducibility of tungsten species. On the other hand, we previously monitored the evolution of zirconia–tungstate from an inactive catalytic material to an active one and demonstrated that activity correlated with the presence of strong Brønsted acid sites (10). In this study, we also associated a decrease in specific activity with a reduction in surface Brønsted acid strength. So even though we cannot exclude the role of redox chemistry in our samples, there is compelling evidence that Brønsted acidity remains a key indicator of catalytic activity.

CONCLUSIONS

The addition of silica stabilizes zirconia–tungstate against sintering by heat treatment. The resulting increase in surface area requires that tungstate loading be increased over standard loadings, to achieve saturation coverage of the surface for activity in *n*-butane isomerization. On poorly mixed zirconia–silica, tungstate remains dispersed on the mixed oxide surface, which consists largely of silica "patches." Hence, tungstate dispersion does not behave as it would on bulk silica but is stabilized on the silica patches by the underlying zirconia. A reduction in catalytic activity, compared to zirconia–tungstate, demonstrates that dispersed tungstate on silica patches does not stabilize strong acid sites capable of *n*-butane isomerization. Improving mixing by the sol–gel technique of prehydrolysis reduces the segregation of silica on the surface of zirconia. This technique produced the least active material implying that the siloxane species generated by prehydrolysis were the most effective at weakening Brønsted acid strength. Results in this study reaffirmed the key parameters that are crucial in having an active zirconia–tungstate sample and, at the same time, highlight the subtle features that can arise from introducing another dopant to this catalytic system.

ACKNOWLEDGMENT

This work is supported by the Division of Chemical Sciences, Office of Basic Energy Sciences, Office of Energy Research, US Department of Energy (DE-FG02-93ER14345).

REFERENCES

1. Baiker, A., and Kijenski, J., *Catal. Today* **5**, 1 (1989).
2. Tanabe, K., Misono, M., Ono, Y., and Hattori, H., "New Solid Acids and Bases." Elsevier Science, 1989.
3. Ward, D. A., and Ko., E. I., *J. Catal.* **150**, 18 (1994).
4. Song, X., and Sayari, A., *Catal. Rev.-Sci. Eng.* **38**, 329 (1996).
5. Hino, M., and Arata, K., *J. Chem. Soc., Chem. Commun.* 1259 (1987).
6. Hino, M., and Arata, K., *Proc. 9th Inter. Congr. Catal.*, 1727 (1988).
7. Santiesteban, J. G., Vartuli, J. C., Han, S., and Chang, C. D., *J. Catal.* **168**, 431 (1997).
8. Iglesia, E., Barton, D. G., Soled, S. L., Miseo, S., Baumgartner, J. E., Gates, W. E., Fuentes, G. A., and Meitzner, G. D., *Proc. 11th Inter. Congr. Catal.*, 533 (1996).
9. Kim, D. S., Ostromecki, M., and Wachs, I. E., *J. Mol. Catal. A: Chemical* **106**, 93 (1996).
10. Boyse, R. A., and Ko, E. I., *J. Catal.* **171**, 191 (1997).
11. Scheithauer, M., Grasselli, R. K., and Knozinger, H., *Prepr.- Am. Chem. Soc., Div. Pet. Chem.* **42**, 738 (1997).
12. Larsen, G., and Petkovic, L. M., *Appl. Catal. A: General* **148**, 155 (1996).
13. Larsen, G., Lotero, E., Petkovic, L. M., and Shobe, D. S., *J. Catal.* **169**, 67 (1997).
14. Wan, K. T., Khouw, C. B., and Davis, M. E., *J. Catal.* **158**, 199 (1996).
15. Boyse, R. A., and Ko, E. I., *Catal. Lett.* **49**, 17 (1997).
16. Miller, J. B., "Sol-Gel Chemistry as a Synthetic Tool for Studying the Effects of Homogeneity on Mixed Oxide Catalytic Materials," Ph.D. Thesis Dissertation, Carnegie-Mellon University, 1995.
17. Miller, J. B., and Ko, E. I., *J. Catal.* **148**, 673 (1994).

18. Handy, B. E., Baiker, A., Schraml-Marth, M., and Wokaun, A., *J. Catal.* **133**, 1 (1992).
19. Miller, J. B., and Ko, E. I., *Chem. Eng. J.* **64**, 273 (1996).
20. Boyse, R. A., and Ko, E. I., *Catal. Lett.* **38**, 225 (1996).
21. Kataoka, T., and Dumesic, J. A., *J. Catal.* **112**, 66 (1988).
22. Parry, E. P., *J. Catal.* **2**, 371 (1963).
23. Basila, M. R., and Kantner, T. R., *J. Phys. Chem.* **70**, 1681 (1966).
24. Ward, D. A., and Ko, E. I., *Chem. Mater.* **5**, 956 (1993).
25. Larsen, G., Raghavan, S., Marquez, M., and Lotero, E., *Catal. Lett.* **37**, 57 (1996).
26. Ward, D. A., and Ko, E. I., *J. Catal.* **157**, 321 (1995).
27. Kim, D. S., Ostromecki, M., and Wachs, I. E., *Catal. Lett.* **33**, 209 (1995).
28. Monaco, S. J., and Ko, E. I., *Chem. Mater.* **9**, 2404 (1997).
29. Lee, S. W., and Condrate, R. A. Sr., *J. Mater. Sci.* **23**, 2951 (1988).
30. Larsen, G., Lotero, E., and Parra, R. D., *Proc. 11th Inter. Congr. Catal.*, 543 (1996).